

Research Journal of Pharmaceutical, Biological and Chemical Sciences

A Theoretical Study of the Relationships between Electronic Structure and Inhibition of Tumor Necrosis Factor by Cyclopentenone Oximes.

Juan S. Gómez-Jeria* and Andrés Robles-Navarro.

Quantum Pharmacology Unit, Department of Chemistry, Faculty of Sciences, University of Chile. Las Palmeras 3425, Santiago 7800003, Chile.

ABSTRACT

We present a study of the relationships between the electronic structure and the tumor necrosis factor inhibitory capacity of a group of cyclopentenone oximes derivatives. The electronic structure of all the molecules was calculated within the Density Functional Theory at the B3LYP/6-31g(d,p) level with full geometry optimization. Complementary docking studies were performed for three molecules. We found a statistically significant relationship between the variation of the inhibitory capacity and the variation of the values of six local atomic reactivity indices belonging to a common molecular skeleton. A partial inhibitory pharmacophore is proposed. It is shown that there is a surprisingly good qualitative agreement between these results and the docking ones. Also, the most interesting finding is the fact that, when the LMRA equation suggests a particular kind of interaction of an atom with the binding site, docking results suggest that in different molecules this interaction can occur with different residues.

Keywords: Tumor necrosis factor, TNF, QSAR, quantum chemistry, DFT, reactivity indices.

**Corresponding author*

INTRODUCTION

Tumor Necrosis Factor (TNF) (also known as tumor necrosis factor ligand superfamily member 2, TNF alpha, TNF- α , TNF-a DIF, TNFA, TNFSF2, or cachectin) is an inflammatory cytokine having a broad variety of functions [1-10]. TNF is produced by a wide variety of immune and epithelial cell types. It can produce cytotoxicity of certain tumor cell lines, is implicated in the induction of cachexia, is a potent pyrogen and can stimulate cell production and induce cell differentiation under definite conditions. It also contributes to the development of type 2 diabetes through its effects on fatty acid metabolism and insulin resistance. TNF regulates lymphoid tissue development through the control of apoptosis. When TNF is present in excessive concentrations, it is accountable for the destructive inflammatory processes that take place in, for instance, articular cartilage and bone in rheumatoid arthritis. Agents inhibiting the action of TNF might consequently be expected to modify the inflammatory disease process. As examples of anti-TNF drugs we may cite Enbrel (for the treatment of ankylosing spondylitis, juvenile idiopathic arthritis, plaque psoriasis, psoriatic arthritis and rheumatoid arthritis), Remicade (for ankylosing spondylitis, Crohn's disease, plaque psoriasis, psoriatic arthritis, rheumatoid arthritis and ulcerative colitis), Humira (for ankylosing spondylitis, Crohn's disease, juvenile idiopathic arthritis, plaque psoriasis, psoriatic arthritis, rheumatoid arthritis and ulcerative colitis), and Simponi (for ankylosing spondylitis, psoriatic arthritis and rheumatoid arthritis). TNF inhibitors may produce side effects, including some that can be life-threatening. Several TNF inhibitors have been synthesized but it is very necessary to look for new drugs with less unwanted side effects and high *in vivo* TNF inhibitory activity [11-15]. Recently, a series of 3-alkyl-2-aryl-2-cyclopenten-1-one oxime derivatives were synthesized and their TNF inhibitory activity was determined in rat peripheral blood mononuclear cells [16]. In this paper we report the results of a study of the relationships between the electronic structures of the abovementioned molecules and their TNF inhibitory activity. We also carried out complementary docking studies to analyze the mode of binding of three of these molecules with the TNF active site.

METHODS, MODELS AND CALCULATIONS

The same standard procedures used in all our recent research in this field were employed here. Given that they have been widely explained in other papers we present a very short survey. The logarithm of the 50 % inhibitory concentration of TNF ($\log(\text{IC}_{50})$) is related to the local atomic reactivity indices of the cyclopentenone oximes by the following system of linear equations [17-22]:

$$\begin{aligned} \log(\text{IC}_{50}) = & a + \sum_j [e_j Q_j + f_j S_j^E + s_j S_j^N] + \\ & + \sum_j \sum_m [h_j(m) F_j(m) + x_j(m) S_j^E(m)] + \sum_j \sum_{m'} [r_j(m') F_j(m') + t_j(m') S_j^N(m')] + \\ & + \sum_j [g_j \mu_j + k_j \eta_j + o_j \omega_j + z_j \zeta_j + w_j Q_j^{\max}] + \sum_{B=1}^W O_B \end{aligned} \quad (1)$$

where a, e_j, f_j, s_j, h_j etc., are constants to be determined. Eq. 1 contains a set of Local Atomic Reactivity Indices (LARIs) related to charge transfer, electrostatic interactions, orientational effects of the substituents, etc., whose meaning has been discussed in several papers. Table 1 shows a few significant examples.

Table 1: LARIs and their physical interpretation.

LARI	Name	Interpretation	Units
Q_i	Net atomic charge of atom i.	Electrostatic interaction.	e
S_i^E	Total atomic electrophilic superdelocalizability of atom i.	Total electron-donating capacity of atom i.	e/eV
S_i^N	Total atomic nucleophilic superdelocalizability of atom i	Total atomic electron-accepting capacity of atom i.	e/eV
$S_i^E(m)$	Orbital atomic electrophilic superdelocalizability of atom i and occupied MO m.	Electron-donating capacity of atom i at occupied MO m.	e/eV
$S_i^N(m')$	Orbital atomic nucleophilic superdelocalizability of atom i and empty MO m'.	Electron-accepting capacity of atom i at vacant MO m'.	e/eV
F_i	Fukui index of atom i.	Total electron population of atom i.	e
F_{mi}	Fukui index of atom i and occupied MO m.	Electron population of occupied MO m at atom i.	e
$F_{m'i}$	Fukui index of atom i and empty MO m'.	Electron population of vacant MO m' at atom i.	e
μ_i	Local atomic electronic chemical potential of atom i.	HOMO _i *-LUMO _i * midpoint.	eV
η_i	Local atomic hardness of atom i.	HOMO _i *-LUMO _i * gap.	eV
ζ_i	Local atomic softness of atom i.	The inverse of η_i .	1/eV
ω_i	Local atomic electrophilicity of atom i.	Tendency of atom i to receive extra electronic charge together with its resistance to exchange charge with the medium.	eV
Q_i^{\max}	Maximal amount of electronic charge.	Maximal amount of electronic charge that atom i may receive.	---
O_t	Orientalional Parameter of the t-th substituent.	Influences the fraction of molecules attaining the correct orientation to interact with a partner.	uma-Å ²

This model was originally developed to analyze drug-receptor equilibrium constants with excellent results for a wide spectrum of drug-site interactions [20, 23-36]. Recently it was also shown to be very successful when applied to other kinds of biological activities [37-56]. As mentioned above, the biological activity studied here is the inhibition of TNF in rat peripheral blood mononuclear cells by some cyclopentenone oxime derivatives (reported as IC₅₀ in μ M) [16]. The molecules and their TNF inhibitory activity are shown in Fig. 1 and Table 2.

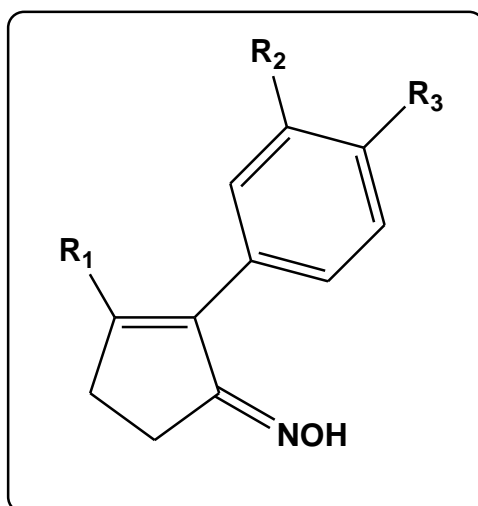
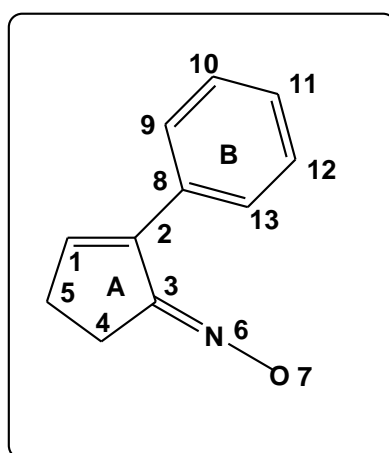

Figure 1: General formula of selected molecules.

Table 2: Molecules and TNF inhibitory activity.

Mol.	R ₁	R ₂	R ₃	log(IC ₅₀)
1	Cyclopentyl	H	F	-0.34
2	Cyclopentyl	F	F	-0.89
3	Cyclopentyl	NO ₂	H	-1.15
4	Cyclopentyl	Methylenedioxy		-0.46
5	Cyclopentyl	OH	H	0.79
6	Cyclopentyl	CF ₃	H	0.49
7	Cyclohexyl	H	F	0.09
8	Cyclohexyl	F	F	-0.47
9	Cyclohexyl	Cl	F	-0.38
10	n-Pentyl	H	F	0.58
11	n-Pentyl	F	F	0.56
12	n-Pentyl	3-Pyridinyl*		1.15
13	n-Butyl	H	F	0.9
14	n-Butyl	Methylenedioxy		0.4
15	n-Propyl	H	F	0.42
16	n-Propyl	F	F	-0.14
17	Ethyl	F	F	0.66
18	Methyl	F	F	1.69

* In this molecule the phenyl ring was replaced by a 3-pyridinyl moiety.

The calculation of the electronic structure was carried out within Density Functional Theory at the B3LYP/6-31G(d,p) level of theory after full geometry optimization. The Gaussian program was employed [57]. The values of the LARIs were calculated with the D-CENT-QSAR software after correcting negative electron populations arising from Mulliken population analysis [58, 59]. Notice that any other population analysis can be employed to calculate the LARIs provided that it will not produce negative electron populations or MO populations greater than 2. We assumed that a set of atoms common to all molecules analyzed (forming a common skeleton) encodes the variation of the biological action all over the series. As the system of linear equations cannot be solved because there are not sufficient molecules, we used Linear Multiple Regression Analysis (LMRA) to detect the atoms and properties involved in the variation of the biological activity. The Statistica software was used for LMRA [60]. The common skeleton numbering is shown in Fig. 2.


Figure 2: Common skeleton with atom numbering.

The docking studies were carried out with Autodock 4 [61, 62]. A crystal structure of TNF was downloaded from the Protein Data Bank (2AZ5) and prepared for use with Autodock. Molecules 1ac, 1cc and 1eb were selected for docking with 2AZ5. All the enzyme residues were kept rigid. A grid box with 66x66x66 points and a grid spacing of 0.375Å were employed. For all procedures, 50 independent runs were performed with an initial population of 300 randomly placed individuals, 50,000,000 energy evaluations and a maximum number of generations of 270,000. The results were clustered based on a 2.0 Å rmsd criterion. The selected structure to discuss was the one having the lowest energy in the largest cluster. It is very important to notice the following fact. On one hand we have an equation relating log(IC₅₀) with the molecules' electronic structures and, on the other, a set of docking results. The equation produced by the LRMA does not contain,

for example, these LARIs that are either constant or without statistical significance. Given that the equation results from a model-based method we hold the thesis that it is more exact than the docking results. Now, if the docking results are in agreement with the LMRA results, they may lead to a more detailed interpretation of these results and they may also provide information about additional interaction sites that cannot be deduced from the equation.

RESULTS

Linear Multiple Regression Analysis.

The best equation obtained is:

$$\log(IC_{50}) = 1.77 - 2.70Q_{12}^{\max} + 1.96F_{12}(HOMO-1)^* - 2.32F_8(HOMO)^* + 0.34S_5^N(LUMO)^* + 2.66F_{11}(HOMO-2)^* - 11.75Q_1 \quad (2)$$

with $n=18$, $R=0.96$, $R^2=0.91$, $\text{adj. } R^2=0.87$, $F(6,11)=19.52$ ($p<0.00003$) and a standard error of estimate of 0.27. No outliers were detected and no residuals fall outside the $\pm 2\sigma$ limits. Here, Q_1 is the net charge of atom 1, Q_{12}^{\max} is the maximal amount of charge atom 12 may receive, $F_{12}(HOMO-1)^*$ is the Fukui index (electron population) of the second highest occupied MO localized on atom 12, $F_8(HOMO)^*$ is the Fukui index of the highest occupied MO localized on atom 8, $F_{11}(HOMO-2)^*$ is the Fukui index of the third highest occupied MO localized on atom 11 and $S_5^N(LUMO)^*$ is the nucleophilic superdelocalizability of the lowest vacant MO localized on atom 5. Tables 3 and 4 display, respectively, the beta coefficients, the results of the t-test for significance of coefficients and the matrix of squared correlation coefficients for the variables appearing in Eq. 2. Table 4 shows that there are no significant internal correlations between independent variables

Table 3: Beta coefficients and t-test for significance of the coefficients in Eq. 2.

	Beta	t(11)	p-level
Q_{12}^{\max}	-0.37	-3.81	<0.003
$F_{12}(HOMO-1)^*$	0.50	5.48	<0.0002
$F_8(HOMO)^*$	-0.31	-3.28	<0.007
$S_5^N(LUMO)^*$	0.39	3.87	<0.003
$F_{11}(HOMO-2)^*$	0.34	3.40	<0.006
Q_1	-0.20	-2.08	<0.06

Table 4: Squared correlation coefficients for the variables appearing in Eq. 2.

	Q_{12}^{\max}	$F_{12}(HOMO-1)^*$	$F_8(HOMO)^*$	$S_5^N(LUMO)^*$	$F_{11}(HOMO-2)^*$
$F_{12}(HOMO-1)^*$	0.05	1.00			
$F_8(HOMO)^*$	0.003	0.01	1.00		
$S_5^N(LUMO)^*$	0.07	0.003	0.04	1.00	
$F_{11}(HOMO-2)^*$	0.005	0.01	0.03	0.09	1.00
Q_1	0.05	0.008	0.0001	0.01	0.05

DOCKING RESULTS

Figures 3, 4 and 5 show, respectively, molecules 3, 12 and 16 docked into the TNF active site. The interactions between atoms are shown with yellow lines. Chimera was used to generate the figures [63]. Table 5 contains a list of the main ligand-residue distances.

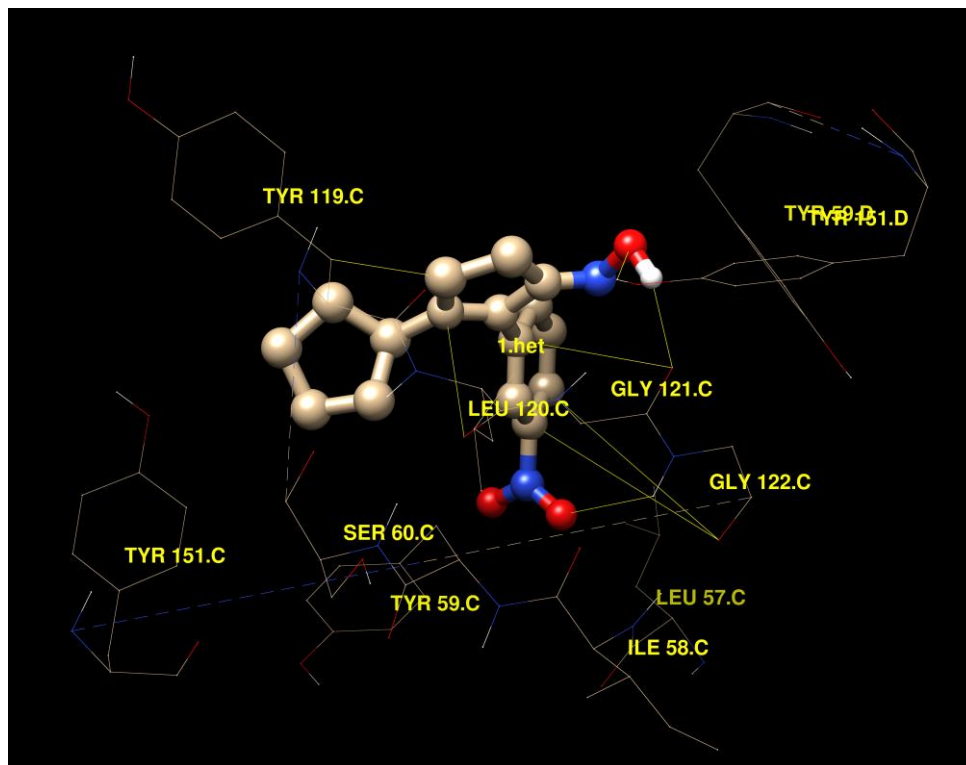


Figure 3: 3 docked into the TNF active site (The letter following the residue's name is the chain ID).

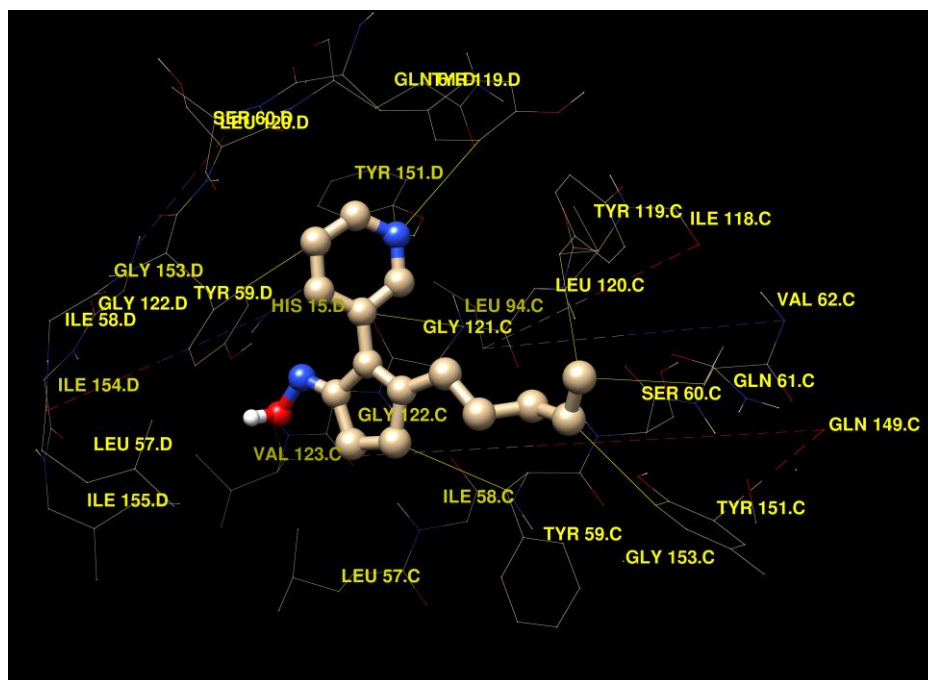


Figure 4: 12 docked into the TNF active site.

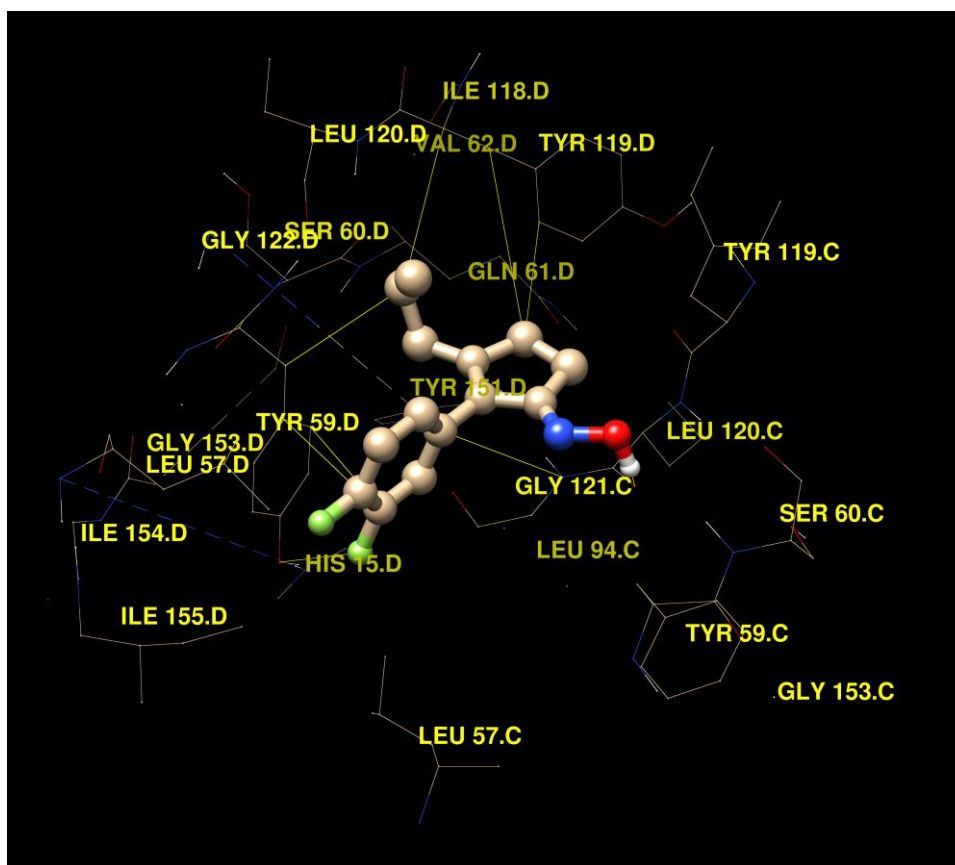


Figure 5: 16 docked into the TNF active site.

Table 5: Main ligand-residue distances.

Mol.	Main interactions (marked in yellow in Figs. 3-5)
3	H (from the NOH moiety)-O from Gly-121C (2.09Å), O (from the NOH moiety)-H from Tyr-151D (2.19Å), C1-O from Leu-120C (3.35Å), C5-C from Tyr-119C (2.99Å), C8-N from Gly-121C (4.61Å), C12-O from Gly-122C (6.00Å), C11-O from Gly-122C (5.42Å), O (from the NO ₂ substituent)-HN from Gly-122C (3.43Å).
12	N (from pyridinyl)-H from Tyr-151D (2.05Å), N (from pyridinyl)-C from Tyr-119D (3.69Å), N (from pyridinyl)-C from Tyr-151D (3.82Å), C12-C from Tyr-151D (3.91Å), C12-C from Tyr-59D (4.52Å), C8-N from Gly-121C (3.50Å), C5-C from Tyr-59C (3.64Å), C (C from the end of n-pentyl chain)-C from Tyr-119C (3.64Å), C (from next to end of n-pentyl chain)-C from Tyr-151C (3.40Å), C (from the end of n-pentyl chain)-C from Gln-61C (3.43Å).
16	H (from the NOH moiety)-O from Gly-121C (1.97Å), C5-C from Tyr-119D (3.28Å), C5-C from Tyr-119D (4.90Å), C12-C from Tyr-59D (3.65Å), C (next to end C of ethyl chain)-C from Tyr-119D (4.41Å), C8-N from Gly-121C (3.91Å), C11-C from Tyr-59D (3.88Å), C5-C from Tyr-159D (3.86Å), F-HO from Tyr-59D (3.74Å).

DISCUSSION

Linear Multiple Regression Analysis

The associated statistical parameters of Eq. 2 show that this equation is statistically significant and that the variation of a set of six local atomic reactivity indices belonging to the common skeleton (see Fig. 2) explains about 87% of the variation of the TNF inhibitory activity. Fig. 6 shows the plot of predicted vs. observed log(IC₅₀) values.

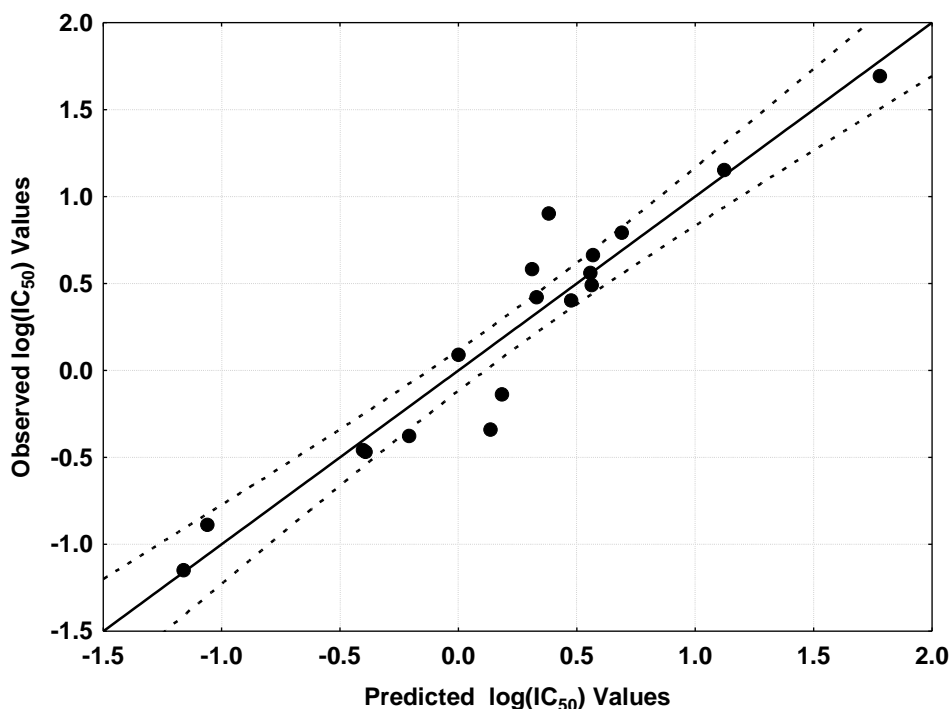


Figure 6: Observed vs. predicted values (Eq. 2) of $\log(IC_{50})$. Dashed lines denote the 95% confidence interval.

We can see in Fig. 6 that three cases lie relatively far from the 95% confidence interval. It is possible that additional molecule-TNF interactions could occur via atoms not belonging to the common skeleton but more experimental results are needed to clarify this point. The beta values (Table 3) indicate that the importance of the variables is $F_{12}(HOMO-1)^* \gg S_5^N(LUMO)^* > Q_{12}^{max} > F_{11}(HOMO-2)^* > F_8(HOMO)^* > Q_1$ (see Fig. 2 for atom numbering). Strong inhibitory activity is associated with high numerical values for Q_{12}^{max} and $F_8(HOMO)^*$, with a positive net charge on atom 1 and with small numerical values for $F_{11}(HOMO-2)^*$, $F_{12}(HOMO-1)^*$ and $S_5^N(LUMO)^*$. A high value for Q_{12}^{max} suggests that atom 12 should be able to accept electrons, i.e., to be a good electrophile. Then it should interact with an electron-rich site (for example an aromatic ring through π - π stacking, an anion, a carbonyl, etc.). Table 5 shows the local MOs of atoms 5, 8, 11 and 12 (Nomenclature: Molecule/ (HOMO-2)* (HOMO-1)* (HOMO)*-(LUMO)* (LUMO+1)* (LUMO+2)*).

Table 5: Local molecular orbital structure of atoms 5, 8, 11 and 12.

Mol.	Atom 5	Atom 8	Atom 11	Atom 12
1	65 σ 66 σ 69- σ 72 σ 73 σ 75 σ	67 π 68 π 69 π -70 π 71 π 72 π	67 π 68 π 69 π -70 π 71 π 72 π	67 π 68 π 69 π -71 π 72 π 73 π
2	69 σ 70 σ 73 σ -77 σ 81 σ 83 σ	70 π 71 π 72 π -74 π 75 π 76 π	71 π 72 π 73 π -74 π 75 π 76 π	70 π 71 π 72 π -74 π 75 π 76 π
3	68 σ 74 σ 76 σ -81 σ 83 σ 85 σ	74 π 75 π 76 π -77 π 78 π 79 π	74 π 75 π 76 π -77 π 78 π 79 π	73 π 74 π 75 π -77 π 78 π 79 π
4	71 σ 73 σ 75 σ -80 σ 81 σ 88 σ	74 π 75 π 76 π -77 π 78 π 79 π	74 π 75 π 76 π -77 π 78 π 79 π	74 π 75 π 76 π -77 π 78 π 79 π
5	65 σ 66 σ 69 σ -73 σ 76 σ 80 σ	67 π 68 π 69 π -70 π 71 π 72 π	67 π 68 π 69 π -70 π 71 π 72 π	66 π 67 π 68 π -71 π 72 π 73 π
6	76 σ 78 σ 81 σ -85 σ 86 σ 91 σ	79 π 80 π 81 π -82 π 83 π 84 π	77 π 80 π 81 π -82 π 83 π 84 π	78 π 79 π 80 π -82 π 83 π 84 π
7	68 σ 70 σ 73 σ -77 σ 78 σ 79 σ	70 π 72 π 73 π -74 π 75 π 76 π	69 π 72 π 73 π -74 π 75 π 76 π	71 π 72 π 73 π -74 π 75 π 76 π
8	72 σ 74 σ 77 σ -81 σ 82 σ 84 σ	74 π 75 π 76 π -79 π 80 π 81 π	69 π 74 π 76 π -78 π 79 π 80 π	74 π 75 π 76 π -78 π 79 π 80 π
9	76 σ 78 σ 81 σ -86 σ 88 σ 90 σ	79 π 80 π 81 π -82 π 83 π 84 π	79 π 80 π 81 π -82 π 83 π 84 π	77 π 78 π 79 π -82 π 83 π 84 π
10	66 σ 67 σ 70 σ -74 σ 75 σ 79 σ	67 π 69 π 70 π -71 π 72 π 73 π	66 π 69 π 70 π -71 π 72 π 73 π	68 π 69 π 70 π -71 π 72 π 73 π
11	70 σ 71 σ 74 σ -78 σ 79 σ 80 σ	72 π 73 π 74 π -75 π 76 π 77 π	72 π 73 π 74 π -75 π 76 π 77 π	71 π 72 π 74 π -75 π 76 π 77 π
12	61 σ 63 σ 66 σ -70 σ 72 σ 74 σ	64 π 65 π 66 π -67 π 68 π 69 π	64 π 65 π 66 π -67 π 68 π 69 π	63 π 64 π 65 π -67 π 68 π 69 π
13	62 σ 63 σ 66 σ -69 σ 70 σ 71 σ	64 π 65 π 66 π -67 π 68 π 69 π	64 π 65 π 66 π -67 π 68 π 69 π	64 π 65 π 66 π -68 π 69 π 70 π
14	67 σ 70 σ 72 σ -77 σ 79 σ 80 σ	71 π 72 π 73 π -74 π 75 π 76 π	71 π 72 π 73 π -74 π 75 π 76 π	69 π 71 π 73 π -74 π 75 π 76 π
15	58 σ 59 σ 62 σ -66 σ 67 σ 71 σ	59 π 61 π 62 π -63 π 64 π 65 π	58 π 61 π 62 π -63 π 64 π 65 π	60 π 61 π 62 π -63 π 64 π 65 π
16	62 σ 63 σ 66 σ -70 σ 71 σ 75 σ	64 π 65 π 66 π -67 π 68 π 69 π	64 π 65 π 66 π -67 π 68 π 69 π	61 σ 62 π 64 π -67 π 68 π 69 π
17	58 σ 59 σ 62 σ -66 σ 67 σ 68 σ	60 π 61 π 62 π -63 π 64 π 65 π	60 π 61 π 62 π -63 π 64 π 65 π	59 π 60 π 62 π -64 π 65 π 66 π
18	54 σ 55 σ 58 σ -61 σ 62 σ 63 σ	56 π 57 π 58 π -59 π 60 π 61 π	56 π 57 π 58 π -59 π 60 π 61 π	55 π 56 π 58 π -60 π 61 π 62 π

A diminished electron population on the $(\text{HOMO}-1)_{12}^*$ will then favor the acceptance of electrons, this being in agreement with the requirement for Q_{12}^{max} . The HOMO^* and $(\text{HOMO}-1)^*$ of atom 12 are of π character in all cases. Fig. 7 shows the local $(\text{HOMO}-1)^*$ of atom 12 in molecules 8 and 13 [64].

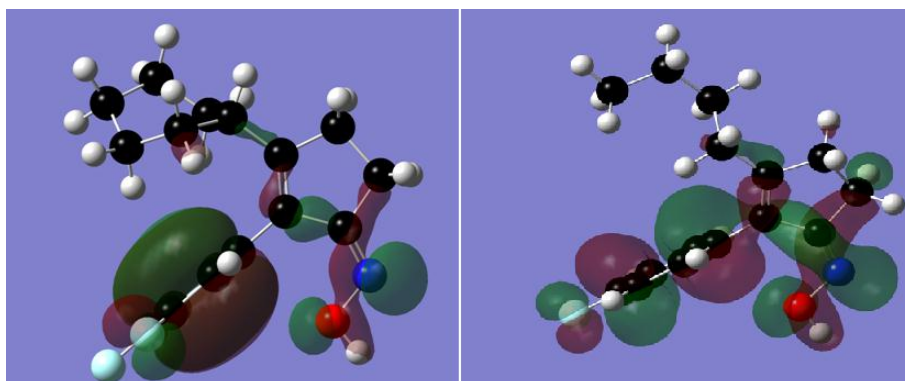


Figure 7: Local $(\text{HOMO}-1)^*$ of atom 12 in molecules 8 (left) and 13 (right). Isovalue of 0.02 e/au^3 .

In the case of molecule 13, the associated Fukui indices of $(\text{HOMO}-1)_{12}^*$ and $(\text{HOMO})_{12}^*$ are, respectively, 0.07 and 0.02. In the case of molecule 8 the corresponding values are 0.36 and 0.05. Therefore, atom 12 should be a better electron acceptor in molecule 8. A small numerical value for $S_5^N(\text{LUMO})^*$ (a positive number in all cases) can be obtained mainly by lowering the LUMO energy which, in turn, raises the electron-accepting capacity of atom 5. Then it is suggested that atom 5 interacts with an electron-rich center. Now, considering that $(\text{LUMO})_5^*$ is of σ nature we propose that this MO is interacting with occupied σ MOs belonging probably to an alkyl chain in the binding site. A high numerical value for $F_8(\text{HOMO})^*$, a π MO in all cases, is obtained by shifting the HOMO energy upwards in the energy axis making atom 8 a better electron donor. This is consistent with the hypothesis of an interaction between atom 8 and an electron-deficient center. $(\text{HOMO}-2)_{11}^*$ is of π nature in all cases and low numerical values are associated with strong inhibitory activity. Considering that $(\text{HOMO}-1)_{11}^*$ and $(\text{HOMO})_{11}^*$ are also of π nature, it is reasonable to suggest that this depletion of electrons could be associated with the interaction with an electron-rich center. In fact atom 11 has a strong positive net charge in all the molecules. The net charge of atom 1 should be positive but, due to its high p value (Table 3), we shall not discuss it. All these suggestions are encompassed in the planar two dimensional (2D) partial pharmacophore shown in Fig. 8.

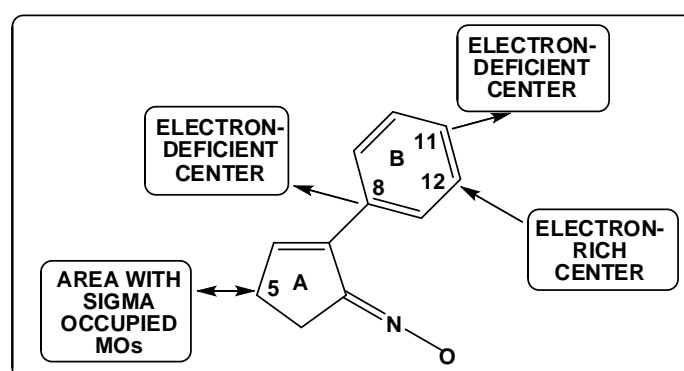


Figure 8: Partial 2D pharmacophore built from Eq. 2.

Molecular electrostatic potential

The molecular electrostatic potential (MEP) map may provide general information about the side from which the molecules approach the site. Figure 9 shows the MEP map of molecules 1, 2, 12 and 14 at isovalues of ± 0.01 . The geometries employed are the *in vacuo* fully optimized ones.

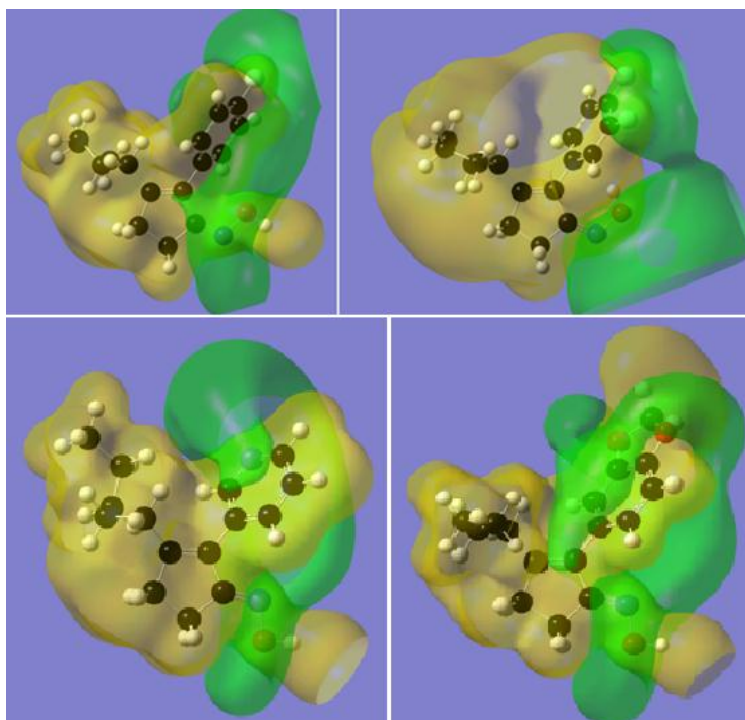


Figure 9: MEP maps of molecules 1 (upper left), 2 (upper right), 12 (lower left) and 14 (lower right). The green isovalue surface corresponds to negative MEP values (-0.01) and the yellow isovalue surface to positive MEP values (0.01).

We can see that at the left side of the molecules positive MEP value volumes predominate. Regarding the right side, the conformation of the NOH moiety influences the appearance or not of a positive MEP region around it. Fig. 10 shows the MEP of molecule 18, the least active one.

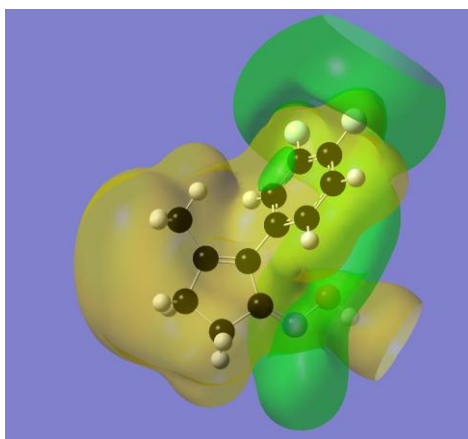


Figure 10: MEP map of molecule 18. The green isovalue surface corresponds to negative MEP values (-0.01) and the yellow isovalue surface to positive MEP values (0.01).

Fig. 10 does not show any particularity distinguishing it from the ones depicted in Fig. 9. It is clear from these figures that it is not possible for the moment to propose correlations between the inhibitory activity and the MEP structure at short distances from the nuclei.

Figure 11 shows the MEP maps of molecules 1, 2, 12 and 14 at 4.5 Å from their nuclei.

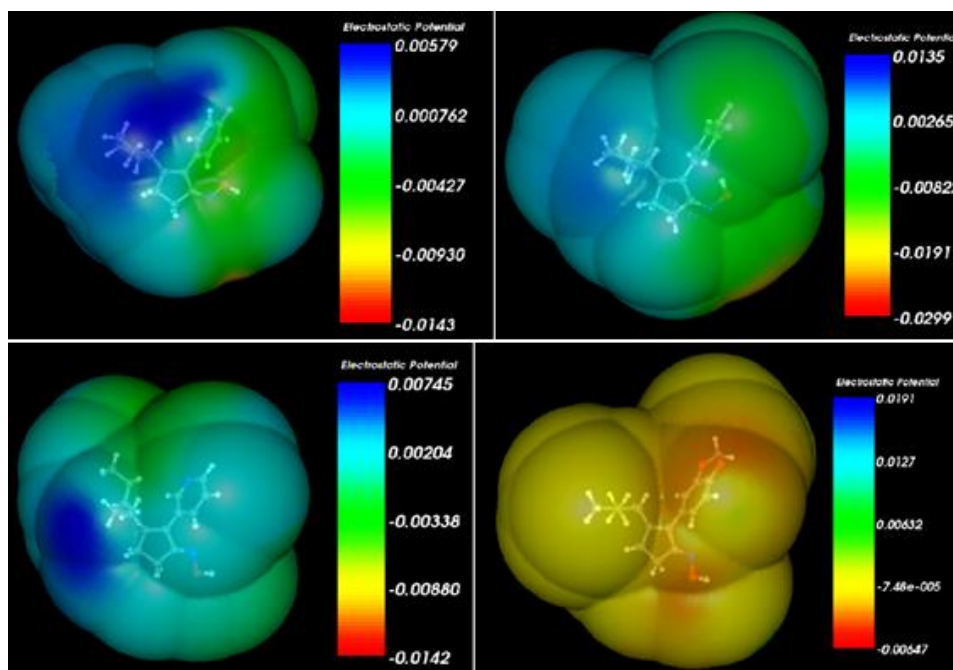


Figure 11: MEP map of molecules 1 (upper left), 2 (upper right), 12 (lower left) and 14 (lower right) at 4.5 Å from the nuclei.

We can see that the main difference in these maps is that molecule 14 is totally surrounded by a negative MEP. Considering that molecules 1, 2 and 12 have negative MEP regions around the phenyl ring (B in Fig. 2), it is possible to suggest that they approach the site with this area facing it. The final reorientation of these molecules seems to occur during the last stages of the binding process. Figure 12 shows the MEP map of molecule 18 at 4.5 Å from the nuclei.

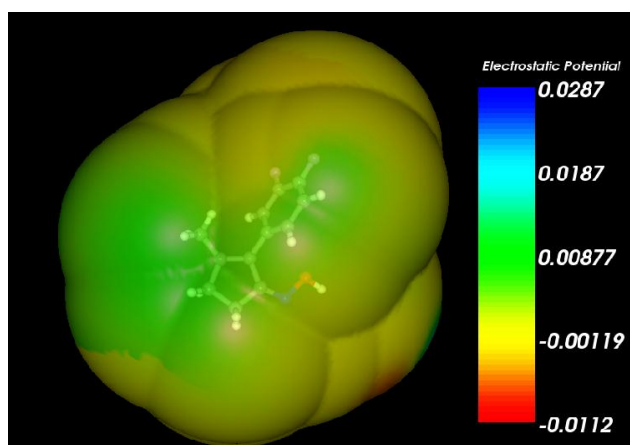


Figure 12: MEP map of molecule 18 at 4.5 Å from the nuclei.

We can see that molecule 18, that possesses the lowest inhibitory potency, has a similar MEP structure.

Conformational flexibility

Figures 13, 14 and 15 show, respectively, the superimposition of the ten lowest energy conformers of molecules 3, 12 and 16. They were calculated with MarvinView (Dreiding force field) and superimposed with Hyperchem. The images were processed with Chimera [63, 65, 66]. Atoms 5, 8 and 11 of Fig. 2 were chosen for the superimposing process. These results must be considered only for a qualitative discussion.

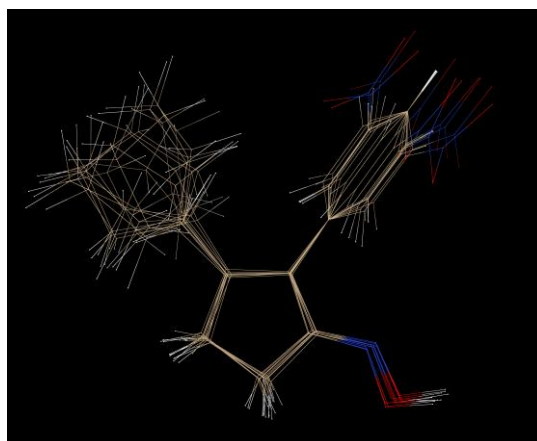


Figure 13: Superimposition of the ten lowest energy conformers of molecule 3.

We can see that in molecule 3 the phenyl ring and the cyclopentyl moieties have enough conformational freedom to reposition themselves for specific interactions with atoms or fragments of the TNF binding site. The NO₂ substituent can adopt at least two positions. This conformational freedom may be limited by high-energy rotation barriers and by the preferential stabilization of one or more conformers by the milieu's microscopic composition.

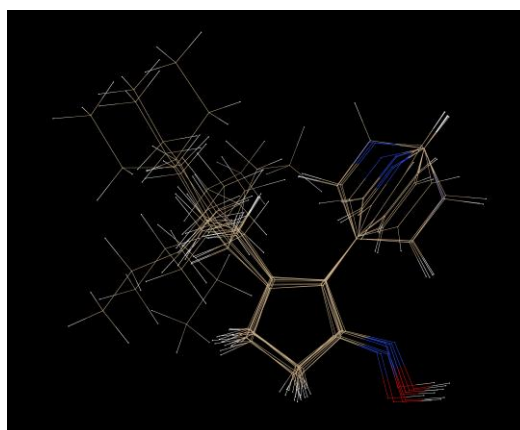


Figure 14: Superimposition of the ten lowest energy conformers of molecule 12.

In the case of molecule 12 we can see that the 3-pyridinyl fragment has a high degree of conformational freedom.

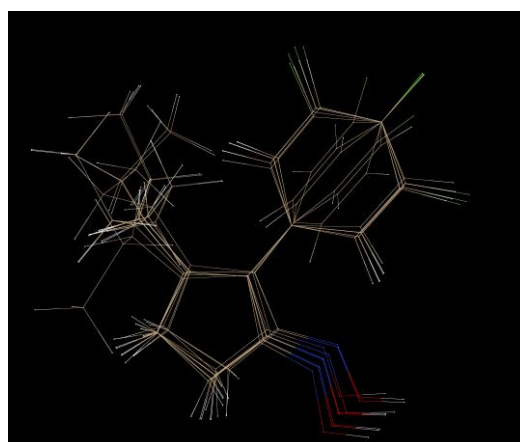


Figure 15: Superimposition of the ten lowest energy conformers of molecule 16.

With molecule 16 we can see that the phenyl ring has a higher degree of conformational freedom than in molecule 3 (Fig. 13). Note that in all three cases the NOH fragment adopts a similar conformation that is different from that found in some fully optimized geometries (compare with Figs. 9-12).

Docking

Making use of the suggestions derived from the LRMA result and the docking results summarized in Table 5, we carried out a comparison shown in Table 6.

Table 6: Possible LRMA and docking results equivalence.

Atom	LRMA	Docking
C5	Interacts with σ occupied MOs	3: σ^* - σ interaction with CH ₂ of Tyr-119C 12: σ^* - σ interaction with CH ₂ of Tyr-59C 16: σ^* - σ interaction with CH ₂ of Tyr-119D
C12	Interacts with an electron-rich center	3: Interaction with O of Gly-122C 12: Interaction with C atoms of aromatic rings of Tyr-151D and Tyr-59D 16: Interaction with C atoms of aromatic ring of Tyr-59D
C11	Interacts with an electron-rich center	3: Interaction with O of Gly-122C 12: Interaction with C atom of aromatic ring of Tyr-119D and Tyr-151D 16: Interaction with C atoms of aromatic ring of Tyr-59D
C8	Interacts with an electron-deficient center	3: Interaction with N of Gly-121C 12: Interaction with N of Gly-122C 16: Interaction with N of Gly-122C
H-bonds of NOH moiety	-----	3: OH...O of Gly-121C O...HO of Tyr-151D 16: OH...O of Gly-121C
NO ₂ of 3	-----	O...HN from Gly-122C
H-bond in 16	-----	F...HO from Tyr-59D
σ - σ interactions	-----	12: C (end of n-pentyl chain)-C from Tyr-119C 12: C (next to end of n-pentyl chain)-C from Tyr-151C 12: C (end of n-pentyl chain)-C from Gln-61C 16: C (next to end of ethyl chain)-C from Tyr-119D

It is worth mentioning that this is the first time that the results of a model-based method are compared with docking results. Considering the number of approximations used to obtain Eq. 1 and the classical mechanical nature of Autodock calculations, the equivalence of both results shown in Table 6 is remarkable. In other works we have found results suggesting that some carbon atoms having only σ MOs localized on them interact with alkyl side chains of the sites. This is the case here for atom C5. We can see in Table 6 and Figs. 3-5 that this atom appears interacting with CH₂ moieties. It was suggested that atom 12 could interact with an electron-rich center. Table 6 shows that C12 effectively interacts with such sites. Interestingly, in molecule 3 atom C12 interacts with an oxygen atom of a glycine, while in molecules 12 and 16 it interacts with carbon atoms belonging to aromatic rings. Both are electron-rich centers but the nature of the interaction seems to be different. This distinction is only possible using Autodock because Eq. 1 is not able to discriminate between both situations. C11 should interact with an electron-rich center. In the case of molecules 12 and 16 this interaction occurs with carbon atoms of phenyl rings of Tyr residues. In the case of molecule 3 an interaction appears with an O atom of a glycine residue. Atom C8 should interact with an electron-deficient center. C8 interacts with a glycine N atom in the three molecules. The most important contribution of docking procedures is their ability to find extra binding sites for atoms not included in the common skeleton. The first example is hydrogen bonding by the NOH moiety: the H atom seems to form H-bonds in molecules 3 and 16. Moreover, in molecule 3 the O atom of NOH seems to engage in a second H-bond. Another example is the H-bond formed by the NO₂ substituent with the NH group of a glycine residue. In the case of molecule 16, a hydrogen bond might form between the fluorine atom and the OH group of a tyrosine residue. Of great importance are the σ - σ interactions between alkyl substituents and methylene moieties of the residues: Autodock detects three such interactions in molecule 12 and one in molecule 16. Some of the aforementioned interactions seem to be of the stacking kind. Recent research on non-covalent interactions involving aromatic rings has shown that the most stable structures are not the sandwich and T-shaped ones [67]. Interestingly, the docking results show that when aromatic rings appear to interact they do not adopt the sandwich or T-

shaped geometries. The hypothesis of the common skeleton is well supported by the LRMA results. We have stated several times that there was a high possibility that in some cases atoms not belonging to that skeleton also interact with a site. This hypothesis has been confirmed for these molecules by the docking results. But the most interesting discovery is the fact that, when the LMRA equation suggests a particular type of interaction of an atom with the binding site, docking results suggest the identity of the interacting partner, and that in different molecules this interaction can occur with different residues.

ACKNOWLEDGEMENTS

Prof. Dr. Bruce K. Cassels (Faculty of Sciences, University of Chile) is thanked for helpful comments.

REFERENCES

- [1] TP Rossard, Tumor necrosis factor, Nova Biomedical Books, New York, 2009.
- [2] JP Waters; JS Pober; JR Bradley, *J. Pathol.*, 2013, 230, 241-248.
- [3] R Perez-Alvarez; M Pérez-de-Lis; M Ramos-Casals; obotBs group, *Curr. Op. Rheumatol.*, 2013, 25, 56-64.
- [4] STC Peake; D Bernardo; ER Mann; HO Al-Hassi; SC Knight; AL Hart, *Inf. Bow. Dis.*, 2013, 19, 1546-1555.
- [5] BE Lippitz, *Lacent Oncol.*, 2013, 14, e218-e228.
- [6] M Cordero-Coma; T Yilmaz; S Onal, *Ocul. Immun. Inflamm.*, 2013, 21, 19-27.
- [7] W-M Chu, *Cancer Lett.*, 2013, 328, 222-225.
- [8] Y Arnsion; D Itzhaky; M Mosseri; V Barak; B Tzur, et al., *Clinic. Rev. Allerg. Immunol.*, 2013, 45, 236-247.
- [9] T Bessissow; M Renard; I Hoffman; S Vermeire; P Rutgeerts; G Van Assche, *Alim. Pharmac. Ther.*, 2012, 36, 312-323.
- [10] C Brightling; L Chachi; D Desai; Y Amrani, "Tumor Necrosis Factor Alpha," in *Inflammation and Allergy Drug Design*, pp. 225-235, Wiley-Blackwell, 2011.
- [11] S Ren; D Hesk; P McNamara; D Koharski; S Borges, *J. Lab. Comp. Radiopharm.*, 2014, 57, 632-636.
- [12] W Lian; P Upadhyaya; CA Rhodes; Y Liu; D Pei, *J. Am. Chem. Soc.*, 2013, 135, 11990-11995.
- [13] M Sharma; S Garigipati; B Kundu; D Vanamala; A Semwal, et al., *Chem. Biol. Drug. Des.*, 2012, 80, 961-970.
- [14] N Gupta; PE Belcher; SA Johnston; CW Diehnelt, *Bioconj. Chem.*, 2011, 22, 1473-1478.
- [15] RJ Cherney; JJW Duan; ME Voss; L Chen; L Wang, et al., *J. Med. Chem.*, 2003, 46, 1811-1823.
- [16] Y Kim; YD Hong; YH Joo; BY Woo; S-Y Kim, et al., *Bioorg. Med. Chem. Lett.*, 2014, 24, 2807-2810.
- [17] JS Gómez-Jeria, *Boll. Chim. Farmac.*, 1982, 121, 619-625.
- [18] JS Gómez-Jeria, *Int. J. Quant. Chem.*, 1983, 23, 1969-1972.
- [19] JS Gómez-Jeria, "Modeling the Drug-Receptor Interaction in Quantum Pharmacology," in *Molecules in Physics, Chemistry, and Biology*, J. Maruani Ed., vol. 4, pp. 215-231, Springer Netherlands, 1989.
- [20] JS Gómez-Jeria; M Ojeda-Vergara; C Donoso-Espinoza, *Mol. Engn.*, 1995, 5, 391-401.
- [21] JS Gómez-Jeria; M Ojeda-Vergara, *J. Chil. Chem. Soc.*, 2003, 48, 119-124.
- [22] JS Gómez-Jeria, *Elements of Molecular Electronic Pharmacology (in Spanish)*, Ediciones Sokar, Santiago de Chile, 2013.
- [23] JS Gómez-Jeria; DR Morales-Lagos, *J. Pharm. Sci.*, 1984, 73, 1725-1728.
- [24] JS Gómez-Jeria; D Morales-Lagos; JI Rodriguez-Gatica; JC Saavedra-Aguilar, *Int. J. Quant. Chem.*, 1985, 28, 421-428.
- [25] JS Gómez-Jeria; D Morales-Lagos; BK Cassels; JC Saavedra-Aguilar, *Quant. Struct.-Relat.*, 1986, 5, 153-157.
- [26] JS Gómez-Jeria; P Sotomayor, *J. Mol. Struct. (Theochem)*, 1988, 166, 493-498.
- [27] JS Gómez-Jeria; M Ojeda-Vergara, *Int. J. Quant. Chem.*, 1997, 61, 997-1002.
- [28] JS Gómez-Jeria; L Lagos-Arancibia, *Int. J. Quant. Chem.*, 1999, 71, 505-511.
- [29] JS Gómez-Jeria; L Lagos-Arancibia; E Sobarzo-Sánchez, *Bol. Soc. Chil. Quím.*, 2003, 48, 61-66.
- [30] JS Gómez-Jeria; F Soto-Morales; G Larenas-Gutierrez, *Ir. Int. J. Sci.*, 2003, 4, 151-164.
- [31] JS Gómez-Jeria; LA Gerli-Candia; SM Hurtado, *J. Chil. Chem. Soc.*, 2004, 49, 307-312.
- [32] F Soto-Morales; JS Gómez-Jeria, *J. Chil. Chem. Soc.*, 2007, 52, 1214-1219.
- [33] JS Gómez-Jeria; F Soto-Morales; J Rivas; A Sotomayor, *J. Chil. Chem. Soc.*, 2008, 53, 1393-1399.
- [34] JS Gómez-Jeria, *J. Chil. Chem. Soc.*, 2010, 55, 381-384.
- [35] T Bruna-Larenas; JS Gómez-Jeria, *Int. J. Med. Chem.*, 2012, 2012 Article ID 682495, 1-16.

- [36] JS Gómez-Jeria, *Der Pharm. Lett.*, 2014, 6., 95-104.
- [37] C Barahona-Urbina; S Nuñez-Gonzalez; JS Gómez-Jeria, *J. Chil. Chem. Soc.*, 2012, 57, 1497-1503.
- [38] DA Alarcón; F Gatica-Díaz; JS Gómez-Jeria, *J. Chil. Chem. Soc.*, 2013, 58, 1651-1659.
- [39] JS Gómez-Jeria, *Canad. Chem. Trans.*, 2013, 1, 25-55.
- [40] JS Gómez-Jeria; M Flores-Catalán, *Canad. Chem. Trans.*, 2013, 1, 215-237.
- [41] A Paz de la Vega; DA Alarcón; JS Gómez-Jeria, *J. Chil. Chem. Soc.*, 2013, 58, 1842-1851.
- [42] I Reyes-Díaz; JS Gómez-Jeria, *J. Comput. Methods Drug Des.*, 2013, 3, 11-21.
- [43] JS Gómez-Jeria, *Int. Res. J. Pure App. Chem.*, 2014, 4, 270-291.
- [44] JS Gómez-Jeria, *Brit. Microbiol. Res. J.*, 2014, 4, 968-987.
- [45] JS Gómez-Jeria, *Der Pharma Chem.*, 2014, 6, 64-77.
- [46] JS Gómez-Jeria, *Res. J. Pharmac. Biol. Chem. Sci.*, 2014, 5, 2124-2142.
- [47] JS Gómez-Jeria, *J. Comput. Methods Drug Des.*, 2014, 4, 32-44.
- [48] JS Gómez-Jeria, *Res. J. Pharmac. Biol. Chem. Sci.*, 2014, 5, 424-436.
- [49] JS Gómez-Jeria, *J. Comput. Methods Drug Des.*, 2014, 4, 38-47.
- [50] JS Gómez-Jeria, *Res. J. Pharmac. Biol. Chem. Sci.*, 2014, 5, 780-792.
- [51] JS Gómez-Jeria; J Molina-Hidalgo, *J. Comput. Methods Drug Des.*, 2014, 4, 1-9.
- [52] JS Gómez-Jeria; J Valdebenito-Gamboa, *Der Pharma Chem.*, 2014, 6, 383-406.
- [53] D Muñoz-Gacitúa; JS Gómez-Jeria, *J. Comput. Methods Drug Des.*, 2014, 4, 33-47.
- [54] D Muñoz-Gacitúa; JS Gómez-Jeria, *J. Comput. Methods Drug Des.*, 2014, 4, 48-63.
- [55] DI Pino-Ramírez; JS Gómez-Jeria, *Amer. Chem. Sci. J.*, 2014, 4, 554-575.
- [56] R Solís-Gutiérrez; JS Gómez-Jeria, *Res. J. Pharmac. Biol. Chem. Sci.*, 2014, 5, 1401-1416.
- [57] MJ Frisch; GW Trucks; HB Schlegel; GE Scuseria; MA Robb, et al., *Gaussian98 Rev. A.11.3*, Gaussian, Pittsburgh, PA, USA, 2002.
- [58] JS Gómez-Jeria, *J. Chil. Chem. Soc.*, 2009, 54, 482-485.
- [59] JS Gómez-Jeria, *D-Cent-QSAR: A program to generate Local Atomic Reactivity Indices from Gaussian log files. 1.0*, Santiago, Chile, 2014.
- [60] Statsoft, *Statistica 8.0*, 2300 East 14 th St. Tulsa, OK 74104, USA, 1984-2007.
- [61] GM Morris; R Huey; AJ Olson, "Using AutoDock for Ligand-Receptor Docking," in *Current Protocols in Bioinformatics*, John Wiley & Sons, Inc., 2002.
- [62] GM Morris; R Huey; W Lindstrom; MF Sanner; RK Belew, et al., *J. Comput. Chem.*, 2009, 30, 2785-2791.
- [63] EF Pettersen; TD Goddard; CC Huang; GS Couch; DM Greenblatt, et al., *J. Comput. Chem.*, 2004, 25, 1605-1612.
- [64] RD Dennington; TA Keith; JM Millam, *GaussView 5.0.8*, GaussView 5.0.8, 340 Quinnipiac St., Bldg. 40, Wallingford, CT 06492, USA, 2000-2008.
- [65] Hypercube, *Hyperchem 7.01*, 419 Phillip St., Waterloo, Ontario, Canada, 2002.
- [66] Chemaxon, *MarvinView*, www.chemaxon.com, USA, 2014.
- [67] M Alonso; T Woller; FJ Martín-Martínez; J Contreras-García; P Geerlings; F De Proft, *Chemistry Eur. J.*, 2014, 20, 4931-4941.